

Direct Determination of the Dependence of the Surface Shear and Dilatational Viscosities on the Thermodynamic State of the Interface: Theoretical Foundations

J. M. Lopez^{*,1} and A. Hirsaa[†]

^{*}Department of Mathematics and Earth System Science Center, The Pennsylvania State University, University Park, Pennsylvania 16802; and [†]Department of Mechanical Engineering, Aeronautical Engineering and Mechanics, Rensselaer Polytechnic Institute, Troy, New York 12180-3590

E-mail: lopez@math.la.asu.edu, hirsaa@rpi.edu

Received February 17, 1998; revised June 2, 1998

Recent developments in nonlinear optical techniques for noninvasive probing of a surfactant influenced gas/liquid interface allow for the measurement of the surfactant surface concentration, c , and thus provide new opportunities for the direct determination of its intrinsic viscosities. Here, we present the theoretical foundations, based on the Boussinesq–Scriven surface model without the usual simplification of constant viscosities, for an experimental technique to directly measure the surface shear (μ^s) and dilatational (κ^s) viscosities of a Newtonian interface as functions of the surfactant surface concentration. This ability to directly measure the surfactant concentration permits the use of a simple surface flow for the measurement of the surface viscosities. The requirements are that the interface must be nearly flat, and the flow steady, axisymmetric, and swirling; these flow conditions can be achieved in the deep-channel viscometer driven at relatively fast rates. The tangential stress balance on such an interface leads to two equations; the balance in the azimuthal direction involves only μ^s and its gradients, and the balance in the radial direction involves both μ^s and κ^s and their gradients. By further exploiting recent developments in laser-based flow measuring techniques, the surface velocities and their gradients which appear in the two equations can be measured directly. The surface tension gradient, which appears in the radial balance equation, is incorporated from the equation of state for the surfactant system and direct measurements of the surfactant surface concentration distribution. The stress balance equations are then ordinary differential equations in the surface viscosities as functions of radial position, which can be readily integrated. Since c is measured as a function of radial position, we then have a direct measurement of μ^s and κ^s as functions of c . Numerical computations of the Navier–Stokes equations are performed to determine the appropriate conditions to achieve the requisite secondary flow. © 1998 Academic Press

Key Words: surface dilatational viscosity; surface shear viscosity; Boussinesq–Scriven; nonlinear optics; deep-channel viscometer.

1. INTRODUCTION

The concept of surface (excess) viscosity associated with contaminated gas/liquid interfaces dates back to Plateau (1), and the formal notion of surface viscosity from geometrical and dynamical considerations of an interface characterized by its static equilibrium tension (thermodynamic interfacial tension), σ , and its viscous resistance to motion was expounded by Boussinesq (2). In Boussinesq's treatment, in addition to the surface tension, the interfacial stress is a function of two other intrinsic properties of the interface, the surface shear viscosity, μ^s , and the surface dilatational viscosity, κ^s . Scriven (3) generalized the mathematical description of the mechanics in Boussinesq's treatment and also allowed for time-dependent deformation of the interface. These works have resulted in the formulation of a constitutive relationship for a Newtonian interface, i.e., an interface for which the relationship between the viscous part of surface stress and the surface rate of deformation is linear and the surface shear and dilatational viscosities are independent of the deformation rate, the Boussinesq–Scriven surface model. It is generally recognized that the surface shear and dilatational viscosities are intrinsic to the interface and have a functional dependence on the thermodynamic state of the interface, in particular on the surfactant surface concentration c , and must therefore vanish for $c \rightarrow 0$. Yet, most analyses of interfacial flows only include constant surface viscosities, the so-called constant property formulation. Thus, these models are only valid in systems that can be linearized about an equilibrium state and only the leading order effects of the surface viscosities can be accounted for.

Presently, there are several methods available for the measurement of surface shear viscosity, most of which involve a rotating container of liquid along with some stationary boundaries. Among these, the deep-channel viscometer (4) is widely accepted as the most sensitive and accurate means for measuring μ^s at a given c (5). In this technique, the surface shear viscosity is computed simply from the ratio of the speed of a small seeding particle placed on the interface in the center of an

¹ Present address: Department of Mathematics, Arizona State University, Tempe, AZ 85287-1804.

annular region, with and without surfactant on the interface. Jiang *et al.* (6) have reported consistent measurements of the surface shear viscosity of a given surfactant system using a variety of different techniques. On the other hand, the measurement of surface dilatational viscosity is not straightforward and there are many different approaches to its measurement with widely varying results. Although qualitative agreement has been obtained for a given surfactant using two different techniques (7), there are large discrepancies in the values of the dilatational viscosity at each surfactant concentration, relative differences on the order of 10^5 . It has been conjectured that these discrepancies result from a dependence of κ^s on the surface dilation rate, which was significantly different in the two techniques. However, this is inconsistent with the basic premise of a Newtonian interface for the Boussinesq–Scriven surface model, which was utilized in both techniques. It should be noted that the comparison in Kao *et al.* (7) was between a technique that assumed the constant property formulation for an interface far from equilibrium and another technique that made a quasistatic approximation for a process operating at a cycle rate of order 10 kHz.

There are measurements that suggest that the surface dilatational viscosity may be several orders of magnitude larger than the surface shear viscosity at a given surfactant concentration (8–12) and that both may be of the same order or larger than the viscosity in the bulk multiplied by the pertinent length scale of the bulk flow. Thus, accurate measurements of κ^s based on the Boussinesq–Scriven surface model, without the simplification of constant surface viscosities, are desirable. Descriptions of existing approaches for measuring surface dilatational viscosity are presented in the following section.

2. PRESENTLY USED TECHNIQUES TO DETERMINE THE SURFACE DILATATIONAL VISCOSITY

To measure the dilatation viscosity, the presently available methods include the maximum bubble pressure method (7, 12) and oscillating bubble techniques (13–15). These techniques primarily rely on changes in the surface area of the interface with relatively negligible surface motions. The theories on which the techniques are based are developed in the limit of Stokes flow, where the nonlinear convective terms are negligible compared to the viscous terms. Most are also linearized about an equilibrium state, thereby neglecting variations of the surface viscosities with surfactant concentration. The approximate functional dependence of κ^s on the state of the interface is obtained by measuring κ^s at different surfactant bulk concentrations and then, by assuming various equilibrium models of the transport kinetics, the equilibrium surfactant surface concentration is estimated. However, these theories are strictly only valid for systems not far from equilibrium. These techniques are also complicated by surface dilatational elasticity (Gibbs elasticity) effects when there is change in the surface area due to the expansion (and contraction) of the bubble radius

and subsequent transport of (soluble) surfactant between the interface and the bulk. Unless the *intrinsic* surface dilatational viscosity κ^s is large (e.g., $\kappa^s \geq 1$ g/s is the estimated limit by Johnson and Stebe (13)), these techniques cannot accurately determine κ^s due to the masking effects of Gibbs elasticity, unless, as in the case of the maximum bubble pressure method, the expansion rate of the interface is very large and the surfactant behaves essentially as an insoluble monolayer. Furthermore, Lu and Apfel (16) and Jiang *et al.* (17) explicitly set the interfacial viscosities to zero as they assume that the intrinsic viscous effects will be smaller than the Gibbs elasticity in the range of concentrations considered in their oscillating bubble analysis and electrocapillary wave techniques, respectively. However, their estimates are based on the constant property formulation and the use of particular transport kinetics models.

Apart from the drop deformation methods and the maximum bubble pressure method, measurements of the surface dilatational viscosity have been performed using surface wave methods (5). Since only a small change in the surfactant surface concentration occurs as a result of linear transverse waves, i.e., small-amplitude capillary and capillary–gravity waves, these are generally not very sensitive for the measurement of the intrinsic surface viscosities. Instead, longitudinal waves are utilized in which the amplitude and the phase of a wave generated by the slow (horizontal) movement of a surface-piercing barrier is studied (8, 11, 18). These techniques are related to the approach of Hirska *et al.* (19), who utilized an ascending pair of vortices to produce an unsteady surface flow, since in both cases the interfacial geometry remains unchanged and essentially flat as it is being stretched or compressed.

All the approaches involving bubbles and drops for determining κ^s can only be applied in unsteady processes since they utilize the normal stress balance; if the interface were stationary then the normal stress balance would simply be a hydrostatic balance and κ^s would not be involved. These techniques are only applicable for soluble surfactant systems. This restriction is due not to limitations on the theory, but rather to the practical problems of depositing an insoluble surfactant at the desired concentration level on a bubble, or forming (blowing) a bubble or drop with the desired interfacial state. However, these techniques have the advantage of providing κ^s , unlike the longitudinal wave methods and the vortex pair method which are planar and only provide the combination ($\kappa^s + \mu^s$), thus requiring an independent measure of μ^s at the same thermodynamic state of the interface to determine κ^s . All the present techniques for determining κ^s utilize unsteady processes, whereas most techniques for determining μ^s involve steady flows, and all the techniques for measuring μ^s and κ^s that utilize the tangential stress balance are based on the constant-property formulation.

The present approach for measuring $\mu^s(c)$ and $\kappa^s(c)$ is to utilize the deep-channel viscometer apparatus (Fig. 1), which until now has been used to measure μ^s at a given surfactant concentration, and directly determine μ^s and κ^s by measuring

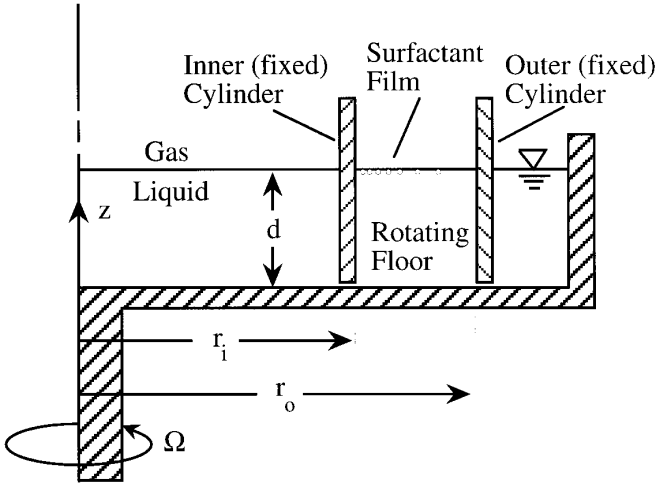


FIG. 1. Schematic of the deep-channel viscometer.

the terms in the tangential stress balances resulting from the Boussinesq–Scriven constitutive relation without assuming that the viscosities are constants. The terms in the stress balance can be determined by measurements of the flow field, performed using noninvasive techniques, such as digital particle image velocimetry (DPIV, e.g., see (20, 21)) or laser-Doppler velocimetry (LDV, e.g., see (22)), and measurements of surfactant surface concentration c . The surfactant surface concentration can be measured directly using nonlinear optical techniques such as second-harmonic generation (SHG, e.g., see (20, 23, 24)). The surfactant surface concentration can then be used to determine the corresponding thermodynamic surface tension, as demonstrated recently by Hirsá *et al.* (19) and Judd (25).

3. CONSTITUTIVE RELATION AND THE STRESS BALANCE AT THE GAS/LIQUID INTERFACE

Scriven (3) and Aris (26) give an account of the force balance at the interface:

$$\begin{aligned}
 & \text{acceleration or inertial force} \\
 &= \text{body force} \\
 &+ \text{surface tension gradient} \\
 &+ \text{viscous resistance to dilation} \\
 &+ \text{viscous resistance to shear} \\
 &+ \text{force due to intrinsic curvature} \\
 &+ \text{force due to movement of the surface.}
 \end{aligned}$$

Here, we are principally interested in determining how the presence of surfactants plays a role in this balance, and as such, we are not interested in the effects of externally imposed body forces. In this formulation, we shall first develop the theory within a framework where the interface is flat. Later, we shall include the effects due to the intrinsic curvature and the motion

of the surface as a small perturbation in the interfacial stress balance.

We begin our treatment of the interface by considering the Boussinesq–Scriven surface fluid model for a Newtonian gas/liquid interface (2, 3, 27), where the surface stress tensor is

$$\mathbf{T}^s = \sigma \mathbf{I}_s + \mathbf{S}^s = (\sigma + (\kappa^s - \mu^s) \text{div}_s \mathbf{u}^s) \mathbf{I}_s + 2\mu^s \mathbf{D}^s,$$

and the viscous part of the surface stress tensor, \mathbf{S}^s , is described as a linear function of the surface rate of deformation tensor

$$2\mathbf{D}^s = \nabla_s \mathbf{u}^s \cdot \mathbf{I}_s + \mathbf{I}_s \cdot (\nabla_s \mathbf{u}^s)^T.$$

In this constitutive equation, κ^s is the surface dilatational viscosity, μ^s is the surface shear viscosity, σ is the thermodynamic (equilibrium) surface tension, \mathbf{u}^s is the surface velocity vector, div_s is the surface divergence operator, ∇_s is the surface gradient operator, and \mathbf{I}_s is the tensor that projects any vector onto the interface.

The surface stress, $\boldsymbol{\tau}$, can then be expressed as (27)

$$\begin{aligned}
 \boldsymbol{\tau} = \nabla_s \cdot \mathbf{T}^s &= \nabla_s \sigma + \nabla_s ((\kappa^s - \mu^s) \text{div}_s \mathbf{u}^s) \\
 &+ 2(\nabla_s \mu^s) \cdot \mathbf{D}^s + 2\mu^s \text{div}_s \mathbf{D}^s.
 \end{aligned}$$

The components of $\boldsymbol{\tau}$ tangential to the interface must be balanced by the corresponding components of the stress from the bulk flow at the interface. We make use of the fact that there is no slip at the interface so that the tangential components of velocity are continuous across it. Also, we impose that the flows on the interface and in the bulk are axisymmetric and that the interface coincides with the plane $z = d$ of the cylindrical coordinate system (r, θ, z) , with an associated bulk velocity vector $\mathbf{u} = (u, v, w)$, and on the interface the surface velocity vector is $\mathbf{u}^s = (u, v)$. The stress balance in the azimuthal direction gives

$$\mu \frac{\partial v}{\partial z} = \mu^s \left(\frac{\partial^2 v}{\partial r^2} + \frac{1}{r} \frac{\partial v}{\partial r} - \frac{v}{r^2} \right) + \frac{\partial \mu^s}{\partial r} \left(\frac{\partial v}{\partial r} - \frac{v}{r} \right), \quad [1]$$

and in the radial direction

$$\begin{aligned}
 \mu \frac{\partial u}{\partial z} = \frac{\partial \sigma}{\partial r} + (\kappa^s + \mu^s) \left(\frac{1}{r} \frac{\partial w}{\partial z} + \frac{\partial^2 u}{\partial r^2} + \frac{2}{r} \frac{\partial u}{\partial r} \right) \\
 - \frac{\partial w}{\partial z} \frac{\partial (\kappa^s + \mu^s)}{\partial r} + \frac{2u}{r} \frac{\partial \mu^s}{\partial r}, \quad [2]
 \end{aligned}$$

where μ is the (shear) viscosity of the bulk liquid.

Equations [1] and [2] constitute the interfacial tangential stress boundary conditions for the coupled interfacial/bulk flow. These equations represent the balance of forces on a surface element resulting from viscous traction or shearing

stress from the bulk, surface tension (or surface pressure) gradients, and surface viscosity effects. It is noteworthy that the condition on \mathbf{v} does not include any surface tension gradient or surface dilatational terms, only surface shear viscosity terms.

The use of swirling axisymmetric bulk flows with a flat interface is well established for the measurement of the surface shear viscosity μ^s (e.g., see (5)). The principle behind the most sensitive of these techniques, the deep-channel viscometer (4), is that Eq. [1] only has surface shear viscosity terms, and if the bulk flow in the deep-channel viscometer is in the Stokes flow regime, implying that the rotation rate of the viscometer's floor is slow (≤ 1 rpm), then the secondary flow (u and w) decouples from the primary flow (\mathbf{v}), and only Eq. [1] needs to be considered on the interface. In this limit, a simple relationship is arrived at between the surface shear viscosity, the bulk fluid viscosity, geometric parameters of the viscometer, and the azimuthal component of velocity \mathbf{v} . However, in the Stokes limit, which allows such an analysis, the effects of surface dilatational viscosity are not manifested, since in this limit u and w vanish and all the terms in Eq. [2] are identically zero.

If one relaxes the constraint of Stokes flow, then the advantages of axisymmetric swirling flows for the determination of both μ^s and κ^s become apparent in light of Eqs. [1] and [2]. Of course, the governing equations are now nonlinear. There is a coupling between the primary and the secondary flow, and a simple analysis is no longer possible. The effects of the secondary flow have been noted to become important in deep-channel viscometers, with typical dimensions and water as the bulk fluid, when the rotation rate of the floor exceeds about 2 or 3 rpm (28). However, with the recent developments in experimental methods for the direct measurements of surfactant surface concentration and flow velocity (19, 20), all the surface tension and surface flow terms in Eqs. [1] and [2] can be directly measured. Thus, two ordinary differential equations in μ^s and $(\kappa^s + \mu^s)$ result that are straightforward to integrate.

4. DETERMINATION OF THE INTRINSIC SURFACE VISCOSITIES

Equations [1] and [2] give the tangential stress balance at the interface; these include contributions from the surface tension gradients and the viscous resistance to shear and dilation. By measuring the surfactant surface concentration and the flow velocities and their gradients at the interface, one could solve for $\mu^s(c)$ and $\kappa^s(c)$ from Eqs. [1] and [2]. Preliminary measurements for the sum $(\kappa^s + \mu^s)$ for a planar two-dimensional flow, treating μ^s and κ^s as constant coefficients, and using an insoluble surfactant, have been made by Hirsa *et al.* (19), who used SHG and DPIV, illustrating the utility of these types of noninvasive measurements. Here, we provide the theoretical formulation to extend their technique to the general case of variable surface viscosities that are functions of the thermody-

namic state of the interface and to variable degrees of surfactant solubility.

Equations [1] and [2] are ordinary differential equations in μ^s and κ^s ; putting

$$F(r) = \mu^s(c(r)) \quad \text{and} \quad G(r) = (\kappa^s(c(r)) + \mu^s(c(r)))$$

gives

$$F' + a_1 F = a_2, \quad [3]$$

$$G' + b_1 G = b_2 + b_3 F', \quad [4]$$

where $a_i(r)$ and $b_i(r)$ are "known" (i.e., directly measured to within sharply estimated error bounds) functions of r . Specifically,

$$a_1(r) = \left(\frac{\partial^2 \mathbf{v}}{\partial r^2} + \frac{1}{r} \frac{\partial \mathbf{v}}{\partial r} - \frac{\mathbf{v}}{r^2} \right) / \left(\frac{\partial \mathbf{v}}{\partial r} - \frac{\mathbf{v}}{r} \right),$$

$$a_2(r) = \mu \frac{\partial \mathbf{v}}{\partial z} / \left(\frac{\partial \mathbf{v}}{\partial r} - \frac{\mathbf{v}}{r} \right),$$

$$b_1(r) = - \left(\frac{1}{r} \frac{\partial w}{\partial z} + \frac{\partial^2 u}{\partial r^2} + \frac{2}{r} \frac{\partial u}{\partial r} \right) / \frac{\partial w}{\partial z},$$

$$b_2(r) = \left(\frac{\partial \sigma}{\partial r} - \mu \frac{\partial u}{\partial z} \right) / \frac{\partial w}{\partial z},$$

$$b_3(r) = \frac{2u}{r} / \frac{\partial w}{\partial z}.$$

For appropriately chosen parameter ranges, the secondary flow in the bulk can produce a surface flow directed radially inward that will clean the surface (i.e., drive $c \rightarrow 0$) in the neighborhood of $r = r_o$, as schematically illustrated in Fig. 1. Thus $F(r_o) = 0$ and $G(r_o) = 0$, providing the initial conditions needed to integrate Eqs. [3] and [4] from $r = r_o$ to $r = r_i$. Equation [3] must be integrated first to get $F(r) = \mu^s(c(r))$, which is then substituted into Eq. [4] and integrated to give $G(r)$. Finally, $G(r) - F(r) = \kappa^s(c(r))$, and since $c(r)$ is directly measured, $\kappa^s(c)$ and $\mu^s(c)$ are obtained.

At steady state, nonlinear optical measurements, using for example SHG, can give the concentration $c(r)$ and together with the equation of state, $\sigma(c)$, provide a direct measurement of

$$\frac{\partial \sigma}{\partial r} = \frac{d\sigma}{dc} \frac{\partial c}{\partial r}.$$

Here, $d\sigma/dc$ is computed from the equation of state and evaluated at the local surfactant concentration, and $\partial c/\partial r$ is found by differentiating the measured $c(r)$ with respect to r .

The equation of state, i.e., $\sigma(c)$ at a fixed temperature, for

insoluble surfactant systems can be obtained readily using conventional methods. For example, the Wilhelmy plate method can be used to measure the equilibrium surface tension as the surface concentration is varied quasistatically in a Langmuir trough. This technique provides an accurate equation of state for insoluble surfactants (29). On the other hand, the measurement of the equation of state for soluble systems can pose profound difficulties as the surfactant surface concentration cannot be measured by conventional probes. Generally, the equation of state is determined indirectly from σ vs bulk concentration, c_b , measurements along with a model constitutive relation, $c(c_b)$, relating the bulk concentration and the equilibrium surface (excess) concentration of surfactant, such as the Langmuir or the Frumkin adsorption isotherms (5). One of the most significant advantages of utilizing the nonlinear optical technique of second-harmonic generation for surfactant measurements is that the SHG signal is generated in the top molecular layer, and thus the technique is extremely surface selective (23, 24). Therefore, the SHG technique may also be utilized to make *direct* measurements of the equation of state for soluble systems.

Since the flow is steady and we can directly measure the surface concentration $c(r)$, the technique described here for measuring both μ^s and κ^s is not restricted to insoluble surfactants, as was the case in Hirsá *et al.* (19) (due to the unsteady nature of their flow), but it is also applicable to the general case of soluble surfactants.

5. ANALYSIS OF THE REQUISITE EXPERIMENTAL FLOW PARAMETERS

To apply the technique of Section 4, the flow must be steady and have a sufficiently strong secondary flow so that at the surface, the radial velocity is strong enough to drive the interface away from its uniform distribution of surfactant. The assumption in the theory for using the deep-channel viscometer to measure μ^s is that if Ω is sufficiently small, then the secondary flow will be negligible so that the radial surface velocity is essentially zero, and hence there are no surfactant surface concentration gradients and $\partial\mu^s/\partial r$ is zero. Experiments suggest that an Ω corresponding to about 2 to 3 rpm is an upper limit (28). Here, we give results from time-dependent axisymmetric Navier–Stokes computations for the deep-channel viscometer geometry in Fig. 1, where we establish the Ω limit of Stokes flow, and determine the maximum surface radial and azimuthal velocities over a wide range of Ω .

The governing equations for flow in the deep-channel viscometer are the axisymmetric Navier–Stokes equations, together with the continuity equation and appropriate boundary and initial conditions. It is convenient to write these using a dimensionless cylindrical polar coordinate system, (R, Θ, Z) , where r_o is the length scale and $1/\Omega$ is the time scale. The corresponding nondimensional velocity vector is $\mathbf{V} = (U, V, W)$ and vorticity vector is $\text{curl}(\mathbf{V}) = (\xi, \eta, \zeta)$. For axisym-

metric flow, there exists a streamfunction, Ψ , such that $U = -1/R\partial\Psi/\partial Z$ and $W = 1/R\partial\Psi/\partial R$. This form of the velocity automatically satisfies the continuity equation.

It should be noted that since the flow is axisymmetric with swirl, it depends only on two spatial coordinates, but consists of velocity components and vorticity components in three orthogonal directions. This should be contrasted with planar two-dimensional flows and axisymmetric flows without swirl, where the velocity vector has only two components and the vorticity vector has only one and is everywhere normal to the velocity. All the techniques previously used to determine κ^s (see Section 2) utilized flows which fall into the latter category. The essential mechanism that we exploit to decouple μ^s from κ^s in the tangential stress balance is the bending of vortex lines at the interface. An example of vortex line bending due to surface shear viscosity was observed experimentally by Hirsá *et al.* (30). In planar two-dimensional flows and axisymmetric flows without swirl, this mechanism is not present, and so the right-hand side of Eq. [1] is identically zero, regardless of the value of μ^s , and only Eq. [2] is dynamically relevant. In the constant-property formulation that is commonly used, Eq. [2] contains viscous effects only in terms of the sum ($\mu^s + \kappa^s$). When the right-hand side of Eq. [1] is different from zero (in particular when $\mu^s \neq 0$) in our axisymmetric flow with swirl, it means that the vortex lines are meeting the surface at some angle different from 90° , and so the two equations, one in terms of μ^s alone and the other in terms of μ^s and κ^s , are both dynamically relevant and the two viscosities can be solved for separately.

The nondimensional axisymmetric Navier–Stokes equations are

$$\begin{aligned} \frac{D\Gamma}{Dt} &= \frac{1}{\text{Re}} \nabla_*^2 \Gamma, \\ \frac{D\eta}{Dt} + \frac{\eta}{R^2} \frac{\partial\Psi}{\partial Z} - \frac{1}{R^3} \frac{\partial\Gamma^2}{\partial Z} &= \frac{1}{\text{Re}} \left(\nabla^2 \eta - \frac{1}{R^2} \frac{\partial\eta}{\partial R} \right), \\ \nabla_*^2 \Psi &= -R\eta, \end{aligned}$$

where

$$\begin{aligned} \frac{D}{Dt} &= \frac{\partial}{\partial t} - \frac{1}{R} \frac{\partial\Psi}{\partial Z} \frac{\partial}{\partial R} + \frac{1}{R} \frac{\partial\Psi}{\partial R} \frac{\partial}{\partial Z}, \\ \nabla^2 &= \frac{\partial^2}{\partial Z^2} + \frac{\partial^2}{\partial R^2} + \frac{1}{R} \frac{\partial}{\partial R}, \\ \nabla_*^2 &= \frac{\partial^2}{\partial Z^2} + \frac{\partial^2}{\partial R^2} - \frac{1}{R} \frac{\partial}{\partial R}, \end{aligned}$$

$\text{Re} = \Omega r_o^2/\nu$ is the Reynolds number, $\nu = \mu/\rho$ is the kinematic viscosity, ρ is the fluid density, and $\Gamma = RV$.

The boundary conditions for the flow in the deep-channel viscometer with a clean, flat surface are as follows: on the stationary cylinder walls ($R = r_i/r_o$ and $R = 1$), $\Psi = 0$, $\Gamma = 0$, and $\eta = -1/R\partial^2\Psi/\partial R^2$; on the rotating floor ($Z = 0$), $\Psi = 0$, $\Gamma = R^2$, and $\eta = -1/R\partial^2\Psi/\partial Z^2$; on the flat, stress-free surface ($Z = d/r_o$), $\Psi = 0$, $\partial\Gamma/\partial Z = 0$, and $\eta = 0$ (this condition neglects the viscosity of air). The initial condition corresponds to a state of rest, and at $t = 0$ the floor is impulsively set to rotate at Ω rad/s; this rate is nondimensionally measured by Re .

The above governing equations are solved using a second-order finite-difference technique in time and space that has been used extensively on related problems without the inner cylinder, i.e., for $r_i = 0$ (31–39).

We utilize the Navier–Stokes computations to determine the parameter space for the experiments. We begin by comparing with a well-established experiment and the Stokes flow theory presented by Mannheimer and Schechter (4).

In (4), experimental measurements of the ratio of the azimuthal velocity at the free surface, $V(R, Z = d/r_o)$, to that at the rotating floor, $V(R, Z = 0) \equiv R$, are presented in their figure 5 for the flow of cetane in a deep-channel viscometer with radius ratio $r_i/r_o = 0.8$, with gap ratio of $d/(r_o - r_i) = 0.690$, and with the floor rotating at 0.986 rpm. In nondimensional terms, this rotation rate corresponds to $Re = 73$. They compared their measurements with Stokes flow theory, where the flow is assumed to be purely in the azimuthal direction. Simple considerations of the vortex dynamics indicate that there must be a secondary flow at any finite Re (e.g., (28)) and that the strength of this secondary flow scales linearly with Re . In Fig. 2, we compare the results of Mannheimer and Schechter with that from our Navier–Stokes computations for the same flow parameters. We should note that the Navier–Stokes computations predict a slightly larger ($\approx 1\%$) azimuthal velocity in the middle of the annulus. A major contribution to this difference is the secondary flow which produces a radial velocity at the surface with a maximum of about 2% of the azimuthal velocity on the surface and is directed radially inward. This radial inflow at the surface convects fluid, which is rotating, from large radius to small radius, and by conservation of angular momentum ($\Gamma = RV$), the azimuthal velocity increases. This secondary flow is neglected in the Stokes flow theory, resulting in a smaller estimate of V . A second factor contributing to the difference between the Navier–Stokes computations and the Stokes flow theory is the drag due to the viscosity of air, which is neglected in the Navier–Stokes computations but included in the Stokes flow theory. However, in this case the ratio of the liquid to gas viscosities is 190:1, so this contribution is an order of magnitude smaller than that due to the secondary flow for this Re .

In addition to requiring a steady, axisymmetric flow with an essentially flat surface to apply the technique of Section 4 to determine both μ^s and κ^s from direct measurements of the flow in a deep-channel viscometer, we also require that the radial

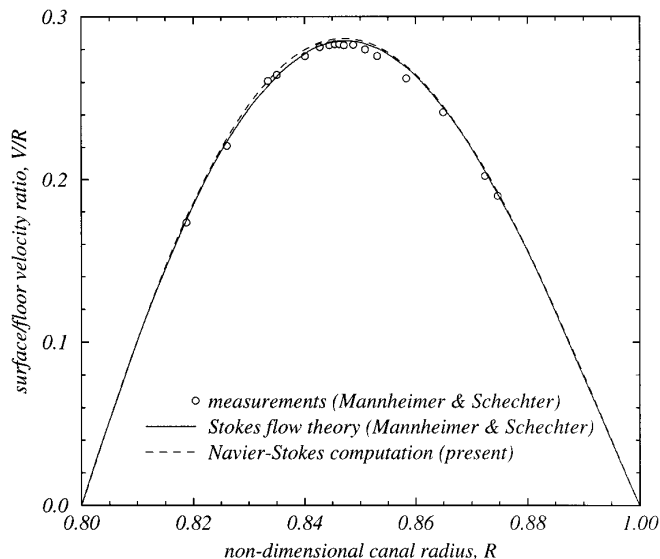


FIG. 2. Comparisons between the measured and computed surface/floor velocity ratio, V/R ; the measurements are those of Mannheimer and Schechter (4) in a deep-channel viscometer with radius ratio $r_i/r_o = 0.80$, depth to gap ratio $d/(r_o - r_i) = 0.690$, and $Re = \Omega r_o^2/\nu r_o^2 = 73$. The Navier–Stokes computation corresponds to the same parameter settings, and the Stokes flow theory curve corresponds to Eq. [21] of (4).

velocity on the surface be sufficiently large compared with the azimuthal velocity. This is needed to produce nonzero terms in Eq. [2]. In the Stokes flow limit, the nondimensional azimuthal velocity is independent of Re and the secondary flow scales linearly with Re . Computations corresponding to the geometry of the deep-channel viscometer in Fig. 1, specifically $r_i/r_o = 0.8$ and $d/(r_o - r_o) = 1.0$, have been performed over a large range in Re ; $1 \leq Re \leq 10^4$. Over this range, the nondimensional time to reach steady state scales linearly with Re . For example, with $Re = 10^3$ and $r_o = 10$ cm, this time is about 500 s for water at room temperature ($\nu \approx 0.01$ cm²/s).

In Figs. 3 and 4, we present computational results that show how the maximum values of V and U on the surface, V_{\max} and U_{\max} , respectively, vary with Re . It is apparent that V_{\max} is independent of Re and that U_{\max} scales linearly with Re for $Re \leq 200$, this being effectively the limit for Stokes-like flow behavior in this geometry. For $Re > 200$, the nonlinear interaction between the primary flow (V) and the secondary flow (U and W) becomes dynamically important. In particular, we note a logarithmic dependence of V_{\max} on Re . This is caused by the radial velocity advecting fluid on the surface radially inward while conserving its angular momentum and thus increasing its azimuthal velocity. We observe that this effect begins to saturate at $Re \approx 10^3$, as further nonlinear interactions alter the flow dynamics. Figure 5 shows the ratio U_{\max}/V_{\max} as a function of Re . At $Re \approx 10^3$, this ratio is about 0.3; the maximum radial velocity is about one-third the maximum azimuthal velocity. The radial velocity for $Re > 10^3$ is strong enough to drive any surface concentration distribution from its equilibrium (uniform) distribution. Of course, the presence of

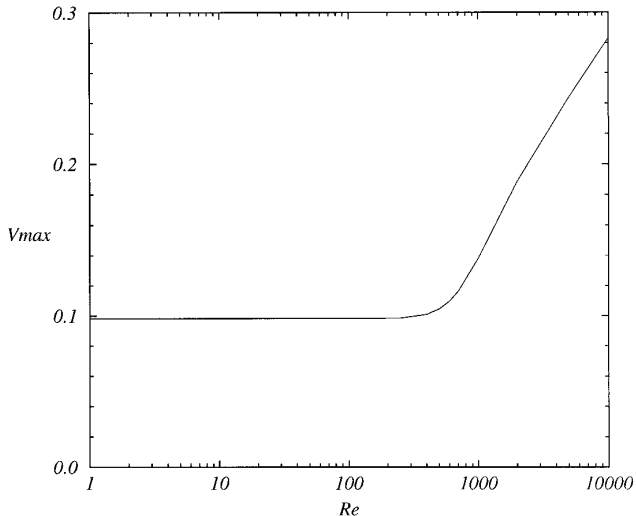


FIG. 3. Variation of V_{\max} , the maximum value of the azimuthal velocity on the surface, with Re , from the Navier–Stokes computations for a deep-channel viscometer with radius ratio $r_i/r_o = 0.8$ and depth to gap ratio $d/(r_o - r_i) = 1$.

surfactant material can be expected to reduce U_{\max} . But our experience with similar flows (37, 39) indicates that the surface velocities will remain adequate.

The above calculations provide guidelines for the selection of parameters for a physical experiment, namely, the rotation rate needed to produce a sufficiently strong secondary flow, and at the same time avoiding the onset of hydrodynamic instability which will occur if the rotation rate is too large. A deep-channel viscometer with outer radius $r_o = 10$ cm, water depth $d = 2$ cm, and a gap $(r_o - r_i) = 2$ cm provides adequate access to the flow region to be interrogated using

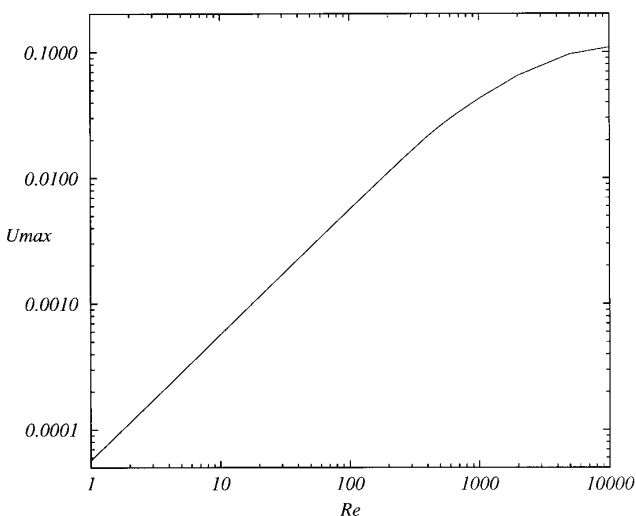


FIG. 4. Variation of U_{\max} , the maximum radial velocity magnitude on the surface, with Re , from the Navier–Stokes computations for a deep-channel viscometer with radius ratio $r_i/r_o = 0.8$ and depth to gap ratio $d/(r_o - r_i) = 1$.

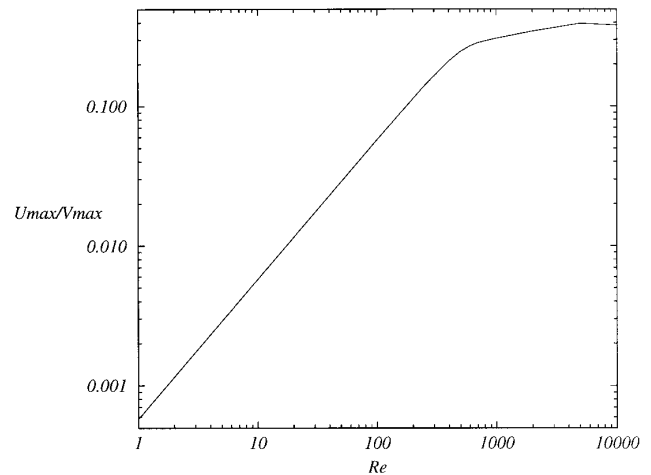


FIG. 5. Variation of U_{\max}/V_{\max} from the Navier–Stokes computations for a deep-channel viscometer with radius ratio $r_i/r_o = 0.8$ and depth to gap ratio $d/(r_o - r_i) = 1$.

optical techniques. The Re required to achieve the desired flow regime for this geometry is $Re \approx 10^{3.5}$. This translates to a rotation rate $\Omega \approx 0.3$ rad/s (≈ 3 rpm). It should be noted that to achieve this Re in a typical deep-channel viscometer, with $r_o = 5$ cm, would require a rotation rate of 12 rpm.

6. GENERALIZATION TO ALLOW FOR SMALL DEFORMATIONS OF THE INTERFACE

For the experimental apparatus (Fig. 1), we can estimate the range of surface deformations by considering the operational range of the governing parameters. The Froude number squared is an estimate of the ratio of surface deformation length scale to the inertial length scale of the flow. In the operational range of the deep-channel viscometer determined in Section 5, the Froude number $Fr = R\Omega/(gd)^{1/2} \sim 0.06$, where g is gravitational acceleration. Thus, the surface deformations will be less than 4×10^{-3} times the radius of the outer annulus with a clean surface. So the expected deformations are certainly small enough to allow us to consider only first-order effects.

Deformations of the interface contribute to the overall force balance which determines the interfacial stress boundary conditions; these consist of a force due to the intrinsic curvature of the interface and another due to its motion. When the interface is flat, its stress balance is given by the tangential components. When it is deforming, the normal stress balance also becomes dynamically important.

In the limit of small deformations, we treat the surface normal as being the normal to the (flat) nondeformed surface, so that to first order, the tangential stresses in the interface (from τ) remain the same as in the flat surface case. The component of the rate of deformation tensor for the bulk flow that balances the radial stress in the interface is now $\mu(\partial u/$

$\partial z + \partial w/\partial r$), since w does not vanish at the deforming interface. This is the only change in the tangential stress balance to first order in the (small) deformation. So, Eq. [1] remains the same and Eq. [2] becomes

$$\mu \left(\frac{\partial u}{\partial z} + \frac{\partial w}{\partial r} \right) = \frac{\partial \sigma}{\partial r} + (\kappa^s + \mu^s) \left(\frac{1}{r} \frac{\partial w}{\partial z} + \frac{\partial^2 u}{\partial r^2} + \frac{2}{r} \frac{\partial u}{\partial r} \right) - \frac{\partial w}{\partial z} \frac{\partial (\kappa^s + \mu^s)}{\partial r} + \frac{2u}{r} \frac{\partial \mu^s}{\partial r}.$$

The only change needed in the determination of μ^s and κ^s as described in Section 4 is to measure $\partial w/\partial r$ at the interface, redefine $b_2(r)$ as

$$b_2(r) = \left(\frac{\partial \sigma}{\partial r} - \mu \left(\frac{\partial u}{\partial z} + \frac{\partial w}{\partial r} \right) \right) / \frac{\partial w}{\partial z},$$

and take the measurements *on* the deformed interface.

Although the analysis for the present technique does not require information about the surface deformation, it should be noted that for a system with constant pressure in the gas phase and negligible gas viscosity, the normal stress balance in the limit of small deformations (where the surface normal is taken to be normal to the nondeformed surface) is (40)

$$-p + \rho gh + 2\mu \frac{\partial w}{\partial z} = 2H\sigma + 2H(\kappa^s + \mu^s)\text{div}_s \mathbf{u}^s,$$

where p is the pressure jump across the interface from gas to liquid; h is the surface elevation relative to the flat, nondeformed surface; and H is the mean curvature which for an axisymmetric system is

$$H = \frac{1}{2} \frac{\partial^2 h}{\partial r^2} \left(1 + \frac{\partial h^2}{\partial r} \right)^{-3/2}.$$

Experimental techniques for the direct measurement of the interfacial velocity on a free surface boundary layer via DPIV have been developed (e.g., (19–21)). Measurements have been taken on flows with comparatively larger Froude numbers than that of the present flow, and the term due to the deformation, $\partial w/\partial r$, has been found to be a small correction to the associated term $\partial u/\partial z$ in b_2 .

Finally, it should be noted that there have been several recent works in which the accuracy and practical limitations of second-harmonic generation for quantitative measurements of surfactant concentration on the air/water interface are described (e.g., (20, 25)). Although the SHG method and other related nonlinear optical methods, such as the sum-frequency generation technique, have been utilized for *in situ* measurements of ocean films as well as laboratory measurements, the

signal-to-noise ratio is relatively small unless the surfactant molecules being probed are resonant at the frequency of the incident laser and/or the second-harmonic light generated at the surface. This can limit the range of surfactant molecules for which detailed measurements can be obtained. However, recent advances in tunable, high-energy, pulsed lasers have extended the applicability of nonlinear optical techniques for quantitative measurements to a wide range of surfactant materials.

7. SUMMARY AND CONCLUSIONS

The theoretical foundations for an experimental method to determine the surface shear and dilatational viscosities, μ^s and κ^s , of a Newtonian gas/liquid interface are established. The formulation treats the surface viscosities as functions of the thermodynamic state of the interface, and, in particular, as functions of the surface concentration of surfactants, c . The flow geometry is that of the familiar deep-channel viscometer, which was originally designed for use in the low-speed, linear regime to measure surface shear viscosity at a given uniform surfactant surface concentration. This same apparatus, when driven faster into the nonlinear regime, produces a strong secondary flow that results in a surface velocity with a significant radial component and a nonuniform distribution of surfactant on the interface. As a result, the tangential surface stress balance in the radial direction becomes dynamically significant, and together with the balance in the azimuthal direction, these provide two ordinary differential equations for μ^s and κ^s . With measurements of the surfactant surface concentration and velocity field, made feasible by modern optical techniques, all of the coefficients in the two ordinary differential equations can be determined, and integration gives $\mu^s(c)$ and $\kappa^s(c)$. We determine the range of parameters required to achieve the requisite secondary flow by the numerical solution of the Navier–Stokes equations. The technique described here for the measurement of $\kappa^s(c)$ and $\mu^s(c)$ is new and complementary to currently available methods.

ACKNOWLEDGMENTS

This work was partially supported by the Office of Naval Research through Grant N000149611063, monitored by Drs. F. L. Herr and D. B. Trizna, and by NSF Grants DMS-9512483, CTS-9803478, and CTS-9803683.

REFERENCES

1. Plateau, J. A. F., *Philos. Mag.* **38**, 445 (1869).
2. Boussinesq, J., *C. R. Hebd. Seances Acad. Sci.* **156**, 983 (1913).
3. Scriven, L. E., *Chem. Eng. Sci.* **12**, 98 (1960).
4. Mannheimer, R. J., and Schechter, R. S., *J. Colloid Interface Sci.* **32**, 195 (1970).
5. Edwards, D. A., Brenner, H., and Wasan, D. T., "Interfacial Transport Processes and Rheology," Butterworth–Heinemann, London, 1991.
6. Jiang, T. S., Chen, J. D., and Slattery, J. C., *J. Colloid Interface Sci.* **96**, 7 (1983).

7. Kao, R. L., Edwards, D. A., Wasan, D. T., and Chen, E., *J. Colloid Interface Sci.* **148**, 247 (1992).
8. Maru, H. C., and Wasan, D. T., *Chem. Eng. Sci.* **34**, 1295 (1979).
9. Djabbarah, N. F., and Wasan, D. T., *Chem. Eng. Sci.* **37**, 175 (1982).
10. Stoodt, T. J., and Slattery, J. C., *AIChE J.* **30**, 564 (1984).
11. Ting, L., Wasan, D. T., Miyano, K., and Xu, S.-Q., *J. Colloid Interface Sci.* **102**, 248 (1984).
12. Avramidis, K. S., and Jiang, T. S., *J. Colloid Interface Sci.* **147**, 262 (1991).
13. Johnson, D. O., and Stebe, K. J., *J. Colloid Interface Sci.* **168**, 21 (1994).
14. Tian, Y., Holt, R. G., and Apfel, R. E., *Phys. Fluids* **7**, 2938 (1995).
15. Nadim, A., in "Third Microgravity Fluid Physics Conference," NASA CP-3338, p. 599 (1996).
16. Lu, H. L., and Apfel, R. E., *J. Colloid Interface Sci.* **134**, 245 (1990).
17. Jiang, Q., Chiew, Y. C., and Valentini, J. E., *J. Colloid Interface Sci.* **155**, 8 (1993).
18. Maru, H. C., Mohan, V., and Wasan, D. T., *Chem. Eng. Sci.* **34**, 1283 (1979).
19. Hirska, A., Korenowski, G. M., Logory, L. M., and Judd, C. D., *Langmuir* **13**, 3813 (1997).
20. Hirska, A., Korenowski, G. M., Logory, L. M., and Judd, C. D., *Exp. Fluids* **22**, 239 (1997).
21. Warnke, A., Gharib, M., and Roesgen, T., *J. Fluids Eng.* **118**, 621 (1996).
22. Bergink-Martens, D. J. M., Bos, H. J., and Prins, A., *J. Colloid Interface Sci.* **165**, 221 (1994).
23. Hicks, J. M., Kennitz, K., Eisenthal, K. B., and Heinz, T. F., *J. Phys. Chem.* **90**, 560 (1986).
24. Shen, Y. R., *Nature* **337**, 519 (1989).
25. Judd, C. D., "Nonlinear Optical Spectroscopy of the Air/Water Interface," Ph.D. thesis, Department of Chemistry, Rensselaer Polytechnic Institute, 1996.
26. Aris, R., "Vectors, Tensors, and the Basic Equations of Fluid Mechanics," Prentice Hall, New York, 1962.
27. Slattery, J. C., "Interfacial Transport Phenomena," Springer-Verlag, Berlin, New York, 1990.
28. Pintar, A. J., Israel, A. B., and Wasan, D. T., *J. Colloid Interface Sci.* **37**, 52 (1971).
29. Gains, G. L., Jr., "Insoluble Monolayers at Liquid-Gas Interfaces," Interscience, New York, 1966.
30. Hirska, A., Harper, J. E., and Kim, S., *Phys. Fluids* **7**, 2532 (1995).
31. Lopez, J. M., *J. Fluid Mech.* **221**, 533 (1990).
32. Brown, G. L., and Lopez, J. M., *J. Fluid Mech.* **221**, 553 (1990).
33. Lopez, J. M., and Perry, A. D., *J. Fluid Mech.* **234**, 449 (1992).
34. Lopez, J. M., *Phys. Fluids* **7**, 2700 (1995).
35. Lopez, J. M., *Phys. Fluids* **8**, 2605 (1996).
36. Lopez, J. M., and Weidman, P. D., *J. Fluid Mech.* **348**, 153 (1996).
37. Lopez, J. M., and Chen, J., in "Proceedings, ASME/OED International Cong. Sym.," Vol. 1, p. 11 (1997).
38. Lopez, J. M., and Shen, J., *J. Comput. Phys.* **139**, 308 (1998).
39. Lopez, J. M., and Chen, J., submitted for publication.
40. Chen, J., "Hydrodynamic Coupling between a Viscoelastic Gas/Liquid Interface and a Swirling Vortex Flow," Ph.D. thesis, Department of Mathematics, The Pennsylvania State University, 1998.